Quantitative Comparison of AIR, SPM, and the Fully Deformable Model for Atlas-Based Segmentation of Functional and Structural MR Images

Minjie Wu,[1] Owen Carmichael,[2,4] Pilar Lopez-Garcia,[5] Cameron S. Carter,[5] and Howard J. Aizenstein[3]*

[1]*Department of Electrical and Computer Engineering, University of Pittsburgh, Pittsburgh, Pennsylvania*
[2]*Department of Radiology, University of Pittsburgh, Pittsburgh, Pennsylvania*
[3]*Department of Psychiatry, University of Pittsburgh, Pittsburgh, Pennsylvania*
[4]*Robotics Institute, Carnegie Mellon University, Pittsburgh, Pennsylvania*
[5]*Department of Psychiatry, University of California at Davis, Davis, California*

Abstract: Typical packages used for coregistration in functional image analyses include automated image registration (AIR) and statistical parametric mapping (SPM). However, both methods have limited-dimension deformation models. A fully deformable model, which combines the piecewise linear registration for coarse alignment with demons algorithm for voxel-level refinement, allows a higher degree of spatial deformation. This leads to a more accurate colocalization of the functional signal from different subjects and therefore can produce a more reliable group average signal. We quantitatively compared the performance of the three different registration approaches through a series of experiments and we found that the fully deformable model consistently produces a more accurate structural segmentation and a more reliable functional signal colocalization than does AIR or SPM. *Hum Brain Mapp 27:747–754, 2006.*

Key words: deformable model; atlas-based segmentation; image registration; fMRI

INTRODUCTION

Accurate region identification is critical for intersubject comparisons of functional brain images, particularly for comparisons across groups. Traditional manual region segmentation is not only labor intensive and time consuming, (to the point of infeasibility with a large dataset and multiple regions), but also introduces human subjectivity and often requires extensive training [Kikinis et al., 1996]. Atlas-based segmentation [Collins et al., 1995; Toga, 1999] overcomes these drawbacks by labeling the anatomical structures for individual brain images, in which the standard labeled atlas brain image is warped to the individual brain image. The anatomical information in the atlas is then carried into the subject space by warping the atlas with the obtained spatial transformation. In this case, the segmentation task is viewed as a registration procedure and the key problem becomes finding the optimal spatial transformation between the template brain image and the individual brain image. Typical packages used for coregistration of neuroimages in func-

Contract grant sponsor: The Pittsburgh Foundation; Contract grant sponsor: Burroughs Wellcome; Contract grant sponsor: NIMH; Contract grant number: K02-MH064190, K23-MH64678, K01-MH01684, P30 MH52247.

*Correspondence to: Howard J. Aizenstein, MD, PhD, Western Psychiatric Institute and Clinic, 3811 O'Hara Street, Pittsburgh, PA 15213. E-mail: aizen@pitt.edu

Received for publication 16 March 2005; Accepted 6 September 2005
DOI: 10.1002/hbm.20216
Published online 6 February 2006 in Wiley InterScience (www.interscience.wiley.com).

tional image analyses are automated image registration [AIR; Woods et al., 1998] and statistical parametric mapping [SPM; Friston et al., 1995]. However, both methods have limited-dimension deformation models: AIR uses a polynomial transformation model with limited coefficients, whereas SPM uses the linear combination of smooth basis functions.

A fully deformable registration technique [Yoo, 2004], which combines the piecewise linear registration for coarse alignment with the demons algorithm [Thirion, 1998] for finer tuning, allows a higher degree of deformation and enables a more accurate spatial deformation field. Recent work from our group has suggested that a similar fully deformable method [Chen, 1999] is more accurate than are affine linear methods at hippocampus segmentation in Alzheimer's disease patients [Carmichael et al., 2005].

In Hellier [2003], several image registration techniques including the demons algorithm, ANIMAL [Collins and Evans 1997], and the optical flow method with a multiresolution and multigrid minimization scheme [Hellier et al., 2001], were evaluated based on their performances at intersubject registration. Unlike the current study, the comparison in Hellier [2003] was restricted to an analysis of anatomic registration and did not address functional imaging data. Previous studies have also looked at the impact of registration on functional imaging data including magnetoencephalography (MEG) data using rigid transformation, piecewise affine transformation, and SPM [Hellier et al., 2002]. A qualitative comparison of registration methods on functional magnetic resonance imaging (fMRI) has also been carried out [Gee et al., 1997], suggesting improvements with a more highly parameterized registration. In the current study, we quantitatively compare the performance of AIR, SPM, and the fully deformable model not only in anatomic space, by comparing the accuracy of the automatic segmented region against the ground-truth region (i.e., hand-drawn region) and the sharpness of the average brain image, but we also extend the comparison into functional space by comparing the effect-size of the colocalized blood oxygenation level-dependent (BOLD) fMRI signal. The deformable registration used here is publicly available (http://www.itk.org), as are AIR and SPM. The Insight Segmentation and Registration Toolkit (ITK) is a collection of C++ registration and segmentation routines developed by the NIH for the medical imaging community; it is freely available and fully supported.

SUBJECTS AND METHODS

Subjects

Ten subjects (7 men; mean age 24.4 years; age range 20–32 years; all right-handed) participated.

Imaging Methods

Scanning was done on a 1.5T Signa scanner (GE Medical Systems, Milwaukee, WI) with 3-D Spoiled Grass (SPGR) (repetition time/echo time [TR/TE] = 5/25 ms, flip angle = 40 degrees, field of view [FOV] = 24 × 18 cm, slice thickness = 1.5 mm, matrix size = 256 × 192). Functional scanning was carried out using a one-shot spiral sequence (TR/TE = 35/2,000 ms, flip angle = 70 degrees, FOV = 24 cm, slice thickness = 3.8 mm, matrix size = 64 × 64 × 26). Subjects carried out eight blocks of a learning task, in which the stimuli appeared in one of four boxes across the screen and the subjects were asked to respond as fast and accurately as possible to the location of the stimuli with a key press (using the index and middle fingers of the both hands). An error for this task is defined as any trial in which the subject pressed the incorrect key while responding to the location of a stimulus. The stimuli appeared once every 2 seconds for 40 seconds, followed by 20 seconds of fixation.

Manual Segmentation of Brain Regions

The standard Montreal Neurological Institute (MNI) brain colin27 [Holmes et al., 1998], which carries high anatomical details and has a high spatial resolution (1 mm^3 voxel size), was used as the template. Two raters manually segmented the right hippocampus and the right anterior cingulate cortex (ACC) on the template colin27, which was used as the atlas in atlas-based automatic segmentation [Lopez-Garcia et al., 2003]. The same two raters also manually classified the right hippocampus and right ACC on each subject, which were used as the ground-truth region mask. The hippocampus was manually traced in the sagittal view. The first medial slice was the one that first showed the cerebral peduncle separated from the upper pons and the most lateral slice was the last showing gray matter from the hippocampus. The posterior limit was set as the slice where an ovoid mass of gray matter started to appear inferiomedially to the trigone of the lateral ventricle. The alveus served as the anterior and superior limit of the head of the hippocampus. ACC tracings were made in serial coronal slices. The sagittal and axial views were used as a reference to outline the ACC. The posterior limit of the ACC was defined by a vertical line perpendicular to the anterior commissure–posterior commissure (AC–PC) plane and passing through the AC. The cingulate and callosal sulci constituted the outer and inner boundary, respectively. When a sulcus running parallel and superior to the cingulate sulcus was present, the paracingulate gyrus was included in the tracing.

Inter-rater reliability for the manual tracings of each one of the two regions of interest (ROIs) was calculated using intraclass correlation coefficient (ICC). The ICCs for the three manually traced ROIs were 0.89 (right hippocampus) and 0.97 (right ACC). To obtain intra-rater reliability a subset of five MR images was retraced by the same rater after 3–4 weeks (mean 22.2 ± 3.4 days). The ICCs for intra-rater reliability were 0.99 (right hippocampus) and 0.93 (right ACC).

Registration Methods

This study evaluates the image registration accuracies of three methods: AIR, SPM, and the fully deformable model. The registration methods were used to coregister the 3D SPGR image of each subject and the template colin27. Before the registration the skull was stripped from both colin27 and the subject's 3D SPGR using the Brain Extraction Tool [BET; Smith 2002]. We chose the AIR registration method, which seemed to produce the best registration accuracy [Lopez-Garcia et al., under review; Rosano et al., 2005]. In this method we used AIR to first perform a 12-parameter affine linear registration, followed by a second-order 30-parameter nonlinear polynomial model. For SPM, we used the standard SPM registration method, which begins with an affine linear registration similar to AIR and then proceeds with a nonlinear registration using a spatial transformation model consisting of a linear combination of low-spatial frequency discrete cosine transform functions. The fully deformable method we used has many degrees of freedom (number of voxels $\times$ 3 $>$ 10^7). This compares to 1,176 degrees of freedom for the SPM registration and 30 degrees of freedom for the registration using AIR. Both methods have lower degrees of freedom and use a limited number of parameters to describe the spatial deformation field; hence, they only allow a certain degree of spatial transformation, which may lead to inaccurate alignment between the individual brain image and the template due to local anatomic variability or pathologic brain changes.

The fully deformable model in this study is similar to that used by Chen [1999]. This was implemented using the registration library in ITK. This method starts with a grid-based piecewise linear registration, and then uses demons registration algorithm as a fine-tuning procedure for a voxel-level spatial deformation. In the demons algorithm, a Guassian smoothing filter is used to smooth the deformation field after each iteration, which is equivalent to an elastic constraint on the deformation. The choice of the standard deviation σ of the Gaussian smoothing kernel is a very important issue, and it has been investigated in previous studies [Cuadra, 2003] that suggested that a typical standard deviation for two healthy brain images to provide a good registration is about 0.5–1 mm. In our model, σ = 1 mm is used. The fully deformable registration, which has many degrees of freedom, allows more spatial deformation, which seems to give it a particular advantage over the other two packages when the brains are much different from the atlas, such as aging brains.

Evaluation Experiments

In this section, we describe the three experiments that were carried out to evaluate the relative accuracies of AIR, SPM, and the fully deformable model. These experiments test the accuracies of registration using: (1) atlas-based segmentation of the hippocampus and anterior cingulate cortex; (2) the smoothness of a mean image generated using the three registration approaches; and (3) the effect-size of the BOLD fMRI signal colocalized across subjects with these registrations.

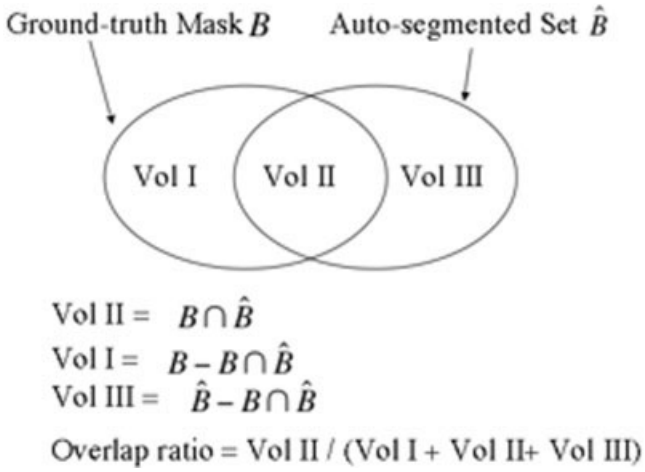

Figure 1.
Illustration of the overlap ratio of automatic segmented region and the hand-drawn ground-truth masks. It is defined as the ratio of overlapping voxels to total voxels.

Experiment 1 (atlas-based segmentation)

In this experiment, the automatic segmented regions are compared, using the overlap ratio, to the manually labeled ground-truth region masks for all 10 subjects. The right hippocampus and right ACC of each subject were estimated through atlas-based segmentation (template→subject registration) with AIR, SPM, and the fully deformable model, respectively. The overlap ratio quantifies how well the automatically segmented anatomical structures overlap with the hand-drawn ground-truth masks. The overlap ratio is defined as the ratio of overlapping voxels to total voxels, as given below (also shown in Fig. 1):

$$\text{overlap ratio} = \frac{\text{vol}\,(B \cap \hat{B})}{\text{vol}[(B - (B \cap \hat{B})) \cup (B \cap \hat{B}) \cup (\hat{B} - (B \cap \hat{B}))]} \quad (1)$$

where B is the ground-truth mask, and $\hat{B}$ is the automatically segmented set.

Experiment 2 (smoothness of mean image)

In Experiment 2, the 10 individual brain images were warped into the template colin27 using each registration approach, and then a mean brain image was created from the resulting warped images. Misalignment or error from the registration leads to a blurred mean brain image. Differences due to variability in individual anatomy also impact

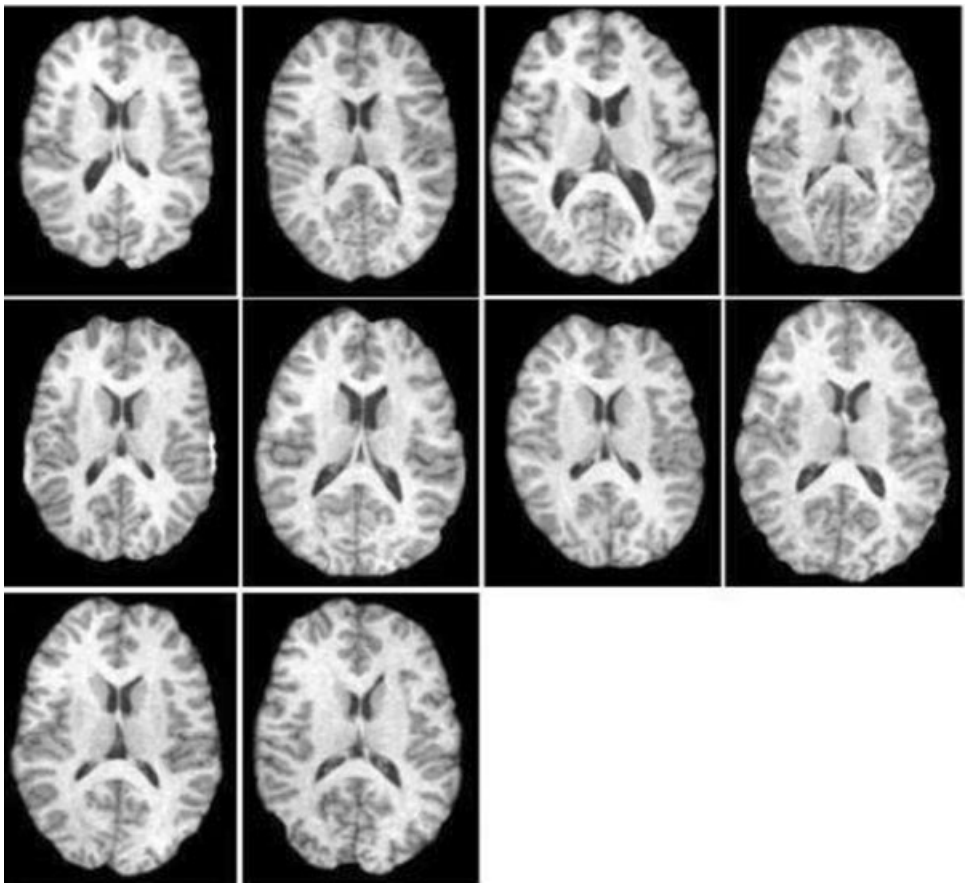

Figure 2.
Ten subject brain images used in the three experiments. Variations in anatomical structures for these subjects can be observed.

registration accuracy. The brain images of the 10 subjects are presented in Figure 2 to show the variability of individual brain anatomy. Visual inspection and quantitative measurement of the spatial correlation (smoothness) of the mean brain image were used to evaluate the registration performance across subjects.

The program 3dFWHM in *AFNI* [Cox, 1996], based on algorithms described by Xiong et al. [1995], provides a way to estimate smoothness of the mean brain images, in which the spatial correlation between voxels along each axis is characterized by full width half maximum (FWHM)x, FWHMy, and FWHMz. By definition, the reported filter width is the estimation of the FWHM of the Gaussian kernel needed to produce the current smoothness; wider FWHM means more smoothness and indicates more inter-subject misalignment during the registrations. The filter widths resulting from 3dFWHM therefore can be used as quantitative smoothness measurements. The 3dFWHM algorithm assumes an isotropic image of random variables, by definition spatially uncorrelated. However, a brain image has spatial correlation. The smoothness estimation of the mean brain images from 3dFWHM therefore includes the inherent spatial correlation of the anatomical images. The smoothness of the anatomical template colin27 was estimated using 3dFWHM and used as the inherent smoothness. The smoothness of the average brain images, generated using AIR, SPM, and the fully deformable model were measured with 3dFWHM and compared to the inherent anatomical smoothness (from colin27).

Experiment 3 (fMRI effect-size)

The registration accuracies from these three approaches were also evaluated by comparing the functional MRI signals acquired on the auto-segmented dorsal anterior cingulate region (dACC). A consistent finding in fMRI studies of cognitive control is that the dACC shows significant activity when subjects make an error or have response conflict during performance of a task [e.g., Carter et al., 1998]. We used a recent fMRI study that we conducted on error and conflict processing [Clark et al., 2002] to examine how the different registration methods differ in their abilities to colocalize across subjects the functional MR signal. In this event-related fMRI study of implicit learning, subjects were asked to press a button as rapidly and accurately as possible based on the position of a stimulus on the screen. Due to the time pressure of the task subjects make on average 20% errors. As expected, we found significant fMRI activation in the dACC on error versus correct trials [Clark et al., under revision]. In the current study, we compare the fidelity of dACC error

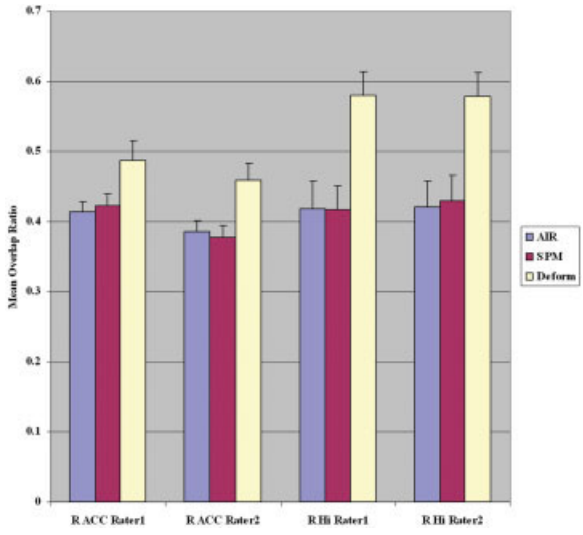

Figure 3.
Mean overlap ratios of right anterior cingulate cortex (R ACC) and right hippocampus (R Hi) across the 10 subjects were generated from atlas-based segmentation with AIR, SPM, and the fully deformable model (Deform). [Color figure can be viewed in the online issue, which is available at www.interscience.wiley.com.]

signal when the dACC was identified using the three different methods: AIR, SPM, and the fully deformable registration. The subjects who participated in the fMRI protocol were 8 of 10 subjects whose structural images were compared in experiments 1 and 2.

The ROI (the dACC taken as the ROI described in Carter et al. [2000]) was automatically segmented using atlas-based segmentation technique (template→subject) with AIR, SPM, and the fully deformable model, for each subject. The signals then were extracted on the segmented dACC after the functional images were aligned to the anatomical images. The fMRI signals were averaged across the ROI to produce an average activation signal across dACC for each trial. Voxel outliers were corrected using the criteria of one standard deviation and the signal was normalized by the first time point at each trial for each voxel. For each subject, the average correct activation time series was generated by averaging the activation time series across the correct trials and the average error activation time series was generated from the error trials, i.e., when the subject inadvertently pressed the incorrect key. The peak activation differences from correct trials versus error trials from all the subjects were statistically examined using a paired two-tailed *t*-test.

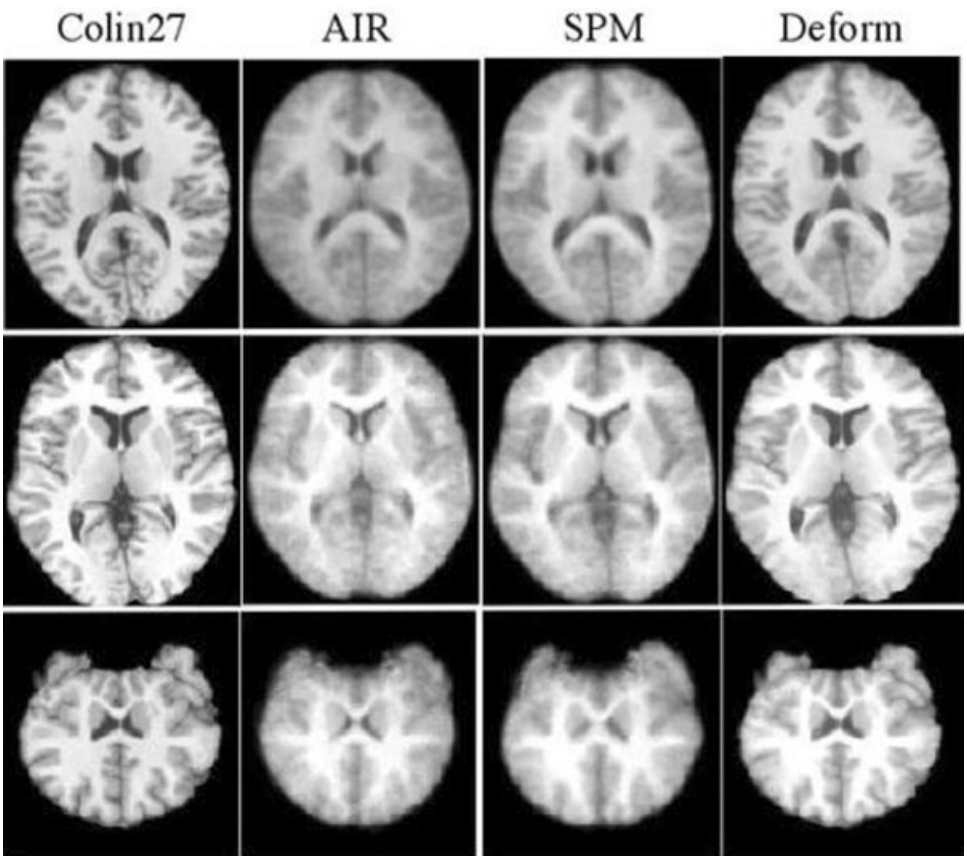

Figure 4.
Mean brain images from the 10 warped subject images (subject→template) using AIR, SPM, and the fully deformable model. The template colin27 is also displayed for comparison.

RESULTS

The results for the three experiments are described in the following sections. As predicted, the fully deformable registration produced better results in all the three experiments.

Experiment 1 (Atlas-Based Segmentation)

The mean overlap ratios across all the subjects for the right hippocampus and the ACC are shown in Figure 3. For both regions, the fully deformable model gives a higher mean overlap ratio than AIR or SPM do, 7.3% higher for right ACC and 15.6% higher for right hippocampus. A paired two-tailed *t*-test of the overlap ratios of the deformable model versus SPM was highly significant at $t(9) = -5.182$, $P = 0.00058$ (right ACC) and $t(9) = -6.372$, $P = 0.00013$ (right hippocampus). Similarly the *t*-test of the overlap ratios of the deformable model against AIR are significant at $t(9) = -3.819$, $P = 0.0041$ (right ACC) and $t(9) = -3.8782$, $P = 0.0037$ (right hippocampus). There was no significant difference in mean overlap ratios between AIR and SPM at $t(9) = 0.0494$, $P = 0.962$ (right ACC) and $t(9) = 0.1853$, $P = 0.857$ (right hippocampus).

Experiment 2 (Smoothness of Mean Image)

For visual inspection, the average brain images from AIR, SPM, and the fully deformable model are shown in Figure 4; the template colin27 is also shown for comparison. As can be seen in Figure 4, the fully deformable model produces a much sharper average brain image with very clear boundaries in which we can clearly identify the cortical sulci and subcortical regions.

The smoothness measurements from 3dFWHM for the average brain images are shown in Table I. As shown in the Table, for the average brain image from the fully deformable model the filter widths along three principal axes resulted from 3dFWHM were very similar to the 3dFWHM results on the template colin27 and were much smaller in all three dimensions than were measurements of mean brain images from AIR or SPM. This indicates that the fully deformable model introduces fewer inter-subject registration errors than do AIR or SPM. The second experiment thus shows the improved performance of the fully deformable method over AIR or SPM at aligning the individual images to the standard MNI reference image.

TABLE I. Smoothness measurements of the averaged warped images

Methods/axes	FWHMx	FWHMy	FWHMz
Colin27(template)	5.31	5.77	5.59
AIR	112.49	128.16	121.98
SPM	121.17	143.85	136.84
Fully deform	5.92	6.57	6.33

The smoothness of averaged warped images from AIR, SPM, and the fully deformable model was measured by the full width half maximum of the Gaussian smoothing filter along *x*, *y*, *z* axes through 3dFWHM. The smoothness of the template was also measured as a comparison, which describes the inherent spatial correlation of the template colin27.

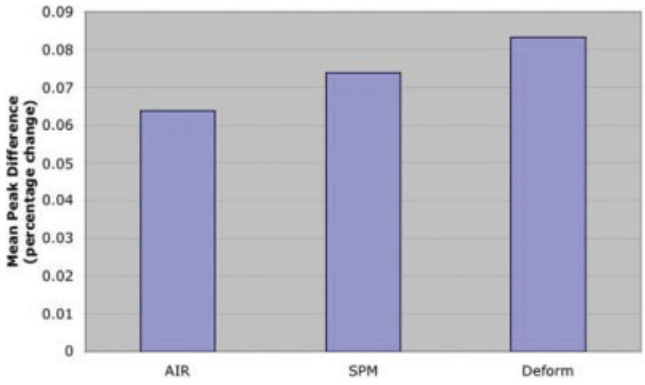

Figure 5.
An average of the peak fMRI activation difference across the eight subjects. For each subject, peak activation difference is the percent signal changes on the correct trials versus error trials. [Color figure can be viewed in the online issue, which is available at www.interscience.wiley.com.]

Experiment 3 (Effect-Size of fMRI Signal)

As predicted there was a greater fMRI signal on the error trials than the correct trials regardless of how the region was segmented (i.e., AIR, SPM, or the fully deformable model). However, as can be seen in Figure 5, with the fully deformable model we extracted higher group difference signals (average signals from error trials − average signals from correct trials) than were extracted from AIR or SPM. As shown in Table II, the paired two-tailed *t*-tests of the eight subjects' peak signals of average time series for correct trials against for error trials was significant at 0.0034 for the fully deformable model, at 0.0295 for AIR and at 0.0668 for SPM, so the *t*-test result were more significant with the fully deformable method, suggesting

TABLE II. Statistical results on fMRI signals

Model	*t*(7)	*P*
AIR	–2.7269	0.0295
SPM	–2.1681	0.0668
Fully deform	–4.3499	0.0034

The paired two-tailed *t*-test results on peak signal of correct time series against peak signal of error time series based on the extracted ROI using AIR, SPM, and the fully deformable model, respectively. AIR, automated image registration; SPM, statistical parametric mapping; Fully Deform, fully deformable model.

a more reliable extraction of the functional imaging signal.

DISCUSSION

In this article, we quantitatively evaluated the coregistration performance of AIR, SPM, and the fully deformable model through a series of experiments. Compared with AIR and SPM, the fully deformable model produced significantly higher overlap ratios for right hippocampus and right anterior cingulate cortex in experiment 1, which demonstrates it can identify ROI more accurately. This leads to a more accurate colocalization of the ROI for functional images, thus it produces more reliable functional signals in experiment 3. Experiments 1 and 3 are based on template→subject coregistration, and experiment 2 is based on subject→template coregistration. In both situations, the fully deformable model shows a better performance compared to that for AIR and SPM in coregistration.

The fully deformable registration is computationally intensive. On a G5 dual-processor Macintosh it took approximately 1 hour per brain, compared to approximately 10 minutes per brain for SPM (on an IRIX 64), and 2 hours for AIR on an IRIX 64. In addition, the registration methods are sensitive to accurate skull stripping. In this study we used BET [Smith, 2002], which was adequate for the 10 subjects in this sample. In other studies, we have found some discrepancies that have led to certain registration inaccuracies. Recently, we have improved the stripping using an automated morphological method [Wu et al., 2005]. This study is limited by a relatively small sample: 10 subjects for the first 2 experiments, and 8 for experiment 3. Nevertheless, the results were significant.

Overall, our results show that the fully deformable registration can improve anatomic alignment of brain images compared to that with SPM and AIR. Moreover, the improved registration seems to lead to a more reliable mean BOLD fMRI signal. Currently, standard fMRI analysis pathways use AIR or SPM. Our results suggest that the fully deformable model could improve the reliability of the colocalized fMRI results; however, this comes at a cost of increased complexity of registration and computation time. Replication of these results in a larger sample is also needed.

ACKNOWLEDGMENTS

This research was supported by the Pittsburgh Foundation, Burroughs Wellcome (Translational Scientist Award to C.S.C.), and the NIMH. We thank the IMAGe (Imaging Methods and Analysis in Geriatrics) group and the Clinical Cognitive Neuroscience Laboratory at the University of Pittsburgh for their assistance.

REFERENCES

Carmichael O, Aizenstein H, Davis S, Becker JT, Thompson P, Meltzer C, Liu Y (2005): Atlas-based hippocampus segmentation in Alzheimer's disease and mild cognitive impairment. Neuroimage 27:979–990.

Carter CS, Braver TS, Barch DM, Botvinick MM, Noll D, Cohen JD (1998): Anterior cingulate cortex, error detection, and the online monitoring of performance. Science 280:747–749.

Carter CS, Macdonald AM, Botvinick M, Ross LL, Stenger VA, Noll D, Cohen JD (2000): Parsing executive processes: strategic vs. evaluative functions of the anterior cingulate cortex. Proc Natl Acad Sci U S A 97:1944–1948.

Chen M (1999): 3-D deformable registration using a statistical atlas with applications in medicine. Robotics Institute Technical Report. Pittsburgh, PA: Carnegie Mellon University.

Clark KA, Aizenstein HJ, Cochran JL, Stenger VA, Carter CS (2002): Conflict monitoring in the absence of awareness: an event-related fMRI study. Presented at the Society for Neuroscience, Orlando, FL, November 2–7, 2002.

Collins DL, Holmes CJ, Peters TM, Evans AC (1995): Automatic 3-D model-based neuroanatomical segmentation. Hum Brain Mapp 3:190–208.

Collins DL, Evans AC (1997): Animal: validation and application of nonlinear registration-based segmentation. Int J Pattern Recogn Artif Intell 8:1271–1294.

Cox RW (1996): AFNI: software for analysis and visualization of functional magnetic resonance neuroimages. Comput Biomed Res 29:162–173.

Cuadra MB (2003): Atlas-based segmentation and classification of magnetic resonance brain images. [PhD dissertation]. Swiss Federal Institute of Technology. Lausanne, Switzerland, November 2003.

Friston KJ, Ashburner J, Frith CD, Poline J-B, Heather JD, Frackowiak RSJ (1995): Spatial registration and normalization of images. Hum Brain Mapp 2:165–189.

Gee JC, Alsop DC, Aguirre GK. 1997: Effect of spatial normalization on analysis of functional data. In: Hanson KM, editor. Medical imaging. Proc SPIE 1997 3034:550–560.

Hellier P, Ashburner J, Corouge I, Barillot C, Friston KJ (2002): Inter-subject registration of functional and anatomical data using SPM. In: 5th International Conference on Medical Image Computing and Computer-Assisted Intervention MICCAI'2002, Lecture Notes in Computer Science, Vol. 2489. Tokyo, Japan, September 2002. p 590–597.

Hellier P, Barillot C, Corouge I, Gibaud B, Le Goualher G, Collins DL, Evans A, Malandain G, Ayache N, Christensen GE, Johnson HJ (2003): Retrospective evaluation of intersubject brain registration. IEEE Trans Med Imaging 22:1120–1130.

Hellier P, Barillot C, Memin E, Perez P (2001): Hierachical estimation of a dense deformation field for 3-D robust registration. IEEE Trans Med Imaging 20:388–402.

Holmes CJ, Hoge R, Collins L, Woods R, Toga AW, Evans AC (1998): Enhancement of MR images using registration for signal averaging. J Comput Assist Tomogr 22:324–333.

Kikinis R, Shenton ME, Iosifescu DV, McCarley RW, Saiviroonporn P, Hokama HH, Robatino A, Metcalf D, Wible CG, Portas CM, Donnino R, Jolesz FA (1996): A digital brain atlas for surgical planning, model-driven segmentation, and teaching. IEEE Trans Vis Comput Graph 2:232–241.

Lopez-Garcia P, Clark KA, Snitz BE, Walter RP, Aizenstein HJ, Carter CS (2003): Automatic MRI-based brain parcellation and

regional volume measurement: a validation study in healthy subjects and individuals with schizophrenia. Presented at the Human Brain Mapping Conference 2003, June 18–22, 2003, New York, NY.

Rosano C, Becker J, Lopez O, Lopez-Garcia P, Carter C, Newman A, Kuller L, Aizenstein H (2005): Morphometric analysis of gray matter volume in demented older adults: exploratory analysis of the cardiovascular health study brain MRI database. Neuroepidemiology 24:221–229.

Smith SM (2002): Fast robust automated brain extraction. Hum Brain Mapp 17:143–155.

Thirion JP (1998): Image matching as a diffusion process: an analogy with Maxwell's demons. Med Image Anal 2:243–260.

Toga AW (1999): Brain Warping. San Diego, CA: Academic Press.

Woods RP, Grafton ST, Watson JD, Sicotte NL, Mazziotta JC (1998): Automated image registration: II. Intersubject validation of linear and nonlinear models. J Comput Assist Tomogr 22:153–165.

Wu M, Rosano C, Aizenstein HJ (2005): A morphological method to improve skull stripping of MR brain images. Presented at the 11th Annual Meeting of the Organization for Human Brain Mapping, 12–16 June 2005, Toronto, Canada.

Xiong J, Gao JH, Lancaster JL, Fox PT (1995): Clustered pixels analysis for functional MRI activation studies of the human brain. Hum Brain Mapp 3:287–301.

Yoo T (2004): Insight into images: principles and practice for segmentation, registration, and image analysis. Wellesey, MA: AK Peters Ltd.